The effect of biological activity, $CaCO_3$ mineral dynamics, and CO_2 degassing in the inorganic carbon cycle in sea ice in late winter-early spring in the Weddell Sea, Antarctica

S. Papadimitriou,[1] H. Kennedy,[1] L. Norman,[1,2] D. P. Kennedy,[1] G. S. Dieckmann,[3] and D. N. Thomas[1,4]

Received 16 March 2012; revised 1 June 2012; accepted 7 June 2012; published 4 August 2012.

[1] A large-scale geographical study of the ice pack in the seasonal ice zone of the Weddell Sea, Antarctica, took place from September to October 2006. Sea ice brines with a salinity greater than 58 and temperature lower than −3.6°C were sampled from 22 ice stations. The brines had large deficits in total alkalinity and in the concentrations of the major dissolved macronutrients (total dissolved inorganic carbon, nitrate, and soluble reactive phosphorus) relative to their concentrations in the surface oceanic water and conservative behavior during seawater freezing. The concentration deficits were related to the dissolved inorganic carbon-consuming processes of photosynthesis, $CaCO_3$ precipitation, and CO_2 degassing. The largest concentration deficits in total dissolved inorganic carbon were found to be associated with $CaCO_3$ precipitation and CO_2 degassing, because the magnitude of the photosynthesis-induced concentration deficit in total dissolved inorganic carbon is controlled by the size of the inorganic nutrient pool, which can be limited in sea ice by its openness to exchange with the surrounding oceanic water.

Citation: Papadimitriou, S., H. Kennedy, L. Norman, D. P. Kennedy, G. S. Dieckmann, and D. N. Thomas (2012), The effect of biological activity, $CaCO_3$ mineral dynamics, and CO_2 degassing in the inorganic carbon cycle in sea ice in late winter-early spring in the Weddell Sea, Antarctica, *J. Geophys. Res.*, *117*, C08011, doi:10.1029/2012JC008058.

1. Introduction

[2] When seawater freezes, the salts and gases dissolved in the parent seawater mass are quantitatively expelled from the ice crystal matrix, raising the ionic strength (salinity) at the ice-seawater interface [*Cox and Weeks*, 1983]. A large part of the expelled dissolved salts escapes the growing ice by gravity drainage into the underlying seawater, contributing to the generation of deep water masses via vertical dense water transport over polar continental shelves [*Toggweiler and Samuels*, 1995; *Anderson et al.*, 2004; *Arrigo et al.*, 2008; *Jutterström and Anderson*, 2010], with the remainder forming the brine in pockets and channels within the sea ice [*Petrich and Eicken*, 2010]. As ice temperature decreases, the salinity of the brine inclusions increases and their size decreases, the latter determining their connectivity within the ice, with the atmosphere above, and with the underlying seawater [*Perovich and Gow*, 1996; *Petrich and Eicken*, 2010]. In turn, this controls the fluxes of dissolved and gaseous substances from consolidated sea ice across its interfaces with the atmosphere and the ocean.

[3] There has been growing interest in sea ice as a significant boundary in the air-sea interaction in polar oceans, through which carbon compounds, among others, transform and migrate, with brine inclusions being the central conduit in this respect [*Loose et al.*, 2011a; *Rysgaard et al.*, 2011; *Geilfus et al.*, 2012]. The exchange of CO_2 between the atmosphere and the upper oceanic waters in ice-covered seas through openings in the ice pack [*Loose and Schlosser*, 2011], such as leads and polynyas, had been thought to be the sole pathway until recently, when a number of studies identified either direct or indirect evidence for exchange between the sea ice and the atmosphere [*Delille et al.*, 2007; *Tison et al.*, 2008; *Loose et al.*, 2011b; *Miller et al.*, 2011; *Geilfus et al.*, 2012]. These advances in our understanding have uncovered the potential for a two-way CO_2 migration over a large expanse (approximately 10%) of the global ocean previously thought to be impervious to such an exchange with the atmosphere.

[4] The concentration gradient across sea ice between the atmospheric and the surface oceanic CO_2 reservoirs in ice-

[1]School of Ocean Sciences, College of Natural Sciences, Bangor University, Anglesey, UK.
[2]Plant Functional Biology and Climate Change Cluster, School of the Environment, University of Technology, Sydney, Broadway, New South Wales, Australia.
[3]Alfred Wegener Institute for Polar and Marine Research, Bremerhaven, Germany.
[4]Marine Research Centre, Finnish Environment Institute, Helsinki, Finland.

Corresponding author: S. Papadimitriou, School of Ocean Sciences, College of Natural Sciences, Bangor University, Menai Bridge, Anglesey LL59 5AB, UK. (s.papadimitriou@bangor.ac.uk)

0148-0227/12/2012JC008058

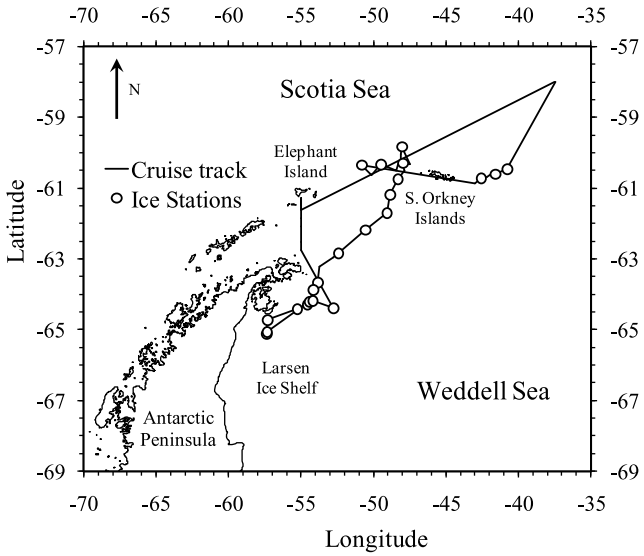

Figure 1. Cruise track and the location of ice stations during the WWOS field study.

covered seas will be modulated by the CO_2 system in the sea ice brine and its continuous adjustment consequent on the biogeochemical processes in this porous medium over seasonal cycles [*Delille et al.*, 2007; *Papadimitriou et al.*, 2007; *Munro et al.*, 2010; *Geilfus et al.*, 2012]. Since the study of polar CO_2 dynamics is in its relative infancy, especially in sea ice-covered regions, it is important to understand the regulatory mechanisms, and their spatial and temporal character in the dynamic physical and biogeochemical environment of sea ice. One such mechanism is CO_2 degassing, documented during the early stages (in the order of 1 month) of sea ice formation and growth under experimental conditions [*Killawee et al.*, 1998; *Papadimitriou et al.*, 2004]. Based on data of total dissolved inorganic carbon (C_T) and its stable isotopic composition ($\delta^{13}C_T$) in natural sea ice in Ross Sea, Antarctica, in late austral spring conditions, this process has been estimated to have been responsible for between 10 and 100% of the C_T concentration deficit seen in the cold upper sea ice layers [*Munro et al.*, 2010]. It has further been calculated that the lower limit of this range would be sufficient to cause a CO_2 efflux from the sea ice-covered polar seas in the order of 0.7 Pg C yr^{-1} [*Munro et al.*, 2010]. Another mechanism is $CaCO_3$ mineral authigenesis in sea ice brines, which affects the parameters of the CO_2 system in the brines, such as total alkalinity (A_T), C_T, and the partial pressure of carbon dioxide (brine pCO_2). The $CaCO_3$ mineral phase has been documented as ikaite in both Arctic and Antarctic pack ice [*Dieckmann et al.*, 2008, 2010], but its formation-dissolution cycle in the polar oceans is still unknown. Finally, biological activity in the many micro-habitats in sea ice cycles carbon and other biophilic elements concentrated in the brines between the mineral and organic reservoirs, causing dramatic changes in the parameters of the CO_2 system, such as pH and brine pCO_2 [*Gleitz et al.*, 1995; *Kennedy et al.*, 2002; *Papadimitriou et al.*, 2007].

[5] The variability in temperature and brine salinity in sea ice is considerable, with large ranges for both parameters over spatial scales, such as with depth in the ice column, and temporally during an annual cycle. These ranges extend from the freezing point of seawater at the ice-seawater interface (−1.85°C at a salinity of 35) to the much colder conditions at the top of ice floes (<−10°C, brine salinity >156). This essentially translates into strong seasonality of the physical, chemical, and biological parameters that regulate the dissolved inorganic carbon species within this idiosyncratic air-sea boundary [*Miller et al.*, 2011; *Geilfus et al.*, 2012]. One step forward would be to translate the measurements of biogeochemical parameters in sea ice, such as dissolved inorganic nutrients and total alkalinity, into potential fluxes of carbon within and out of the sea ice system via the major processes outlined above. This study describes measurements of the concentration of the major dissolved inorganic nutrients and two of the four directly measurable parameters of the CO_2 system in brines from a campaign to the seasonal ice zone (SIZ) in the western Weddell Sea, Antarctica, in the transition from winter to spring. Using this data set, we quantify the relative importance of the biological and abiotic inorganic carbon cycles in sea ice, which was predominantly less than one ice season old.

2. Study Sites

[6] The study was conducted in September and October 2006 during the Winter Weddell Outflow Study (WWOS) onboard *R. V. Polarstern* along an east to west transect between 60° to 61°S and 40° to 52°W, and a northeast to southwest transect between 60°S and 65°S, in the northwestern Weddell Sea [*Lemke*, 2009]. Brine samples and companion ice cores were retrieved at 22 ice stations during a 38-day period (Figure 1). The brine samples were obtained with the sackhole sampling technique [*Gleitz et al.*, 1995; *Papadimitriou et al.*, 2007] by drilling six partial boreholes in a snow-cleared 1 m^2 surface of the sea ice. After allowing the brine from the surrounding sea ice to percolate into the holes, the brine temperature was taken and aliquots for A_T determination were collected in 60 mL borosilicate glass bottles using a plastic syringe and Teflon tubing. Brine aliquots for the measurement of the concentration of the major dissolved inorganic macronutrients (including C_T) were collected and kept in 20 mL plastic syringes to capacity until further processing in the onboard laboratory within 1 h of collection. The aliquots for C_T analysis were filtered through a cellulose nitrate syringe filter (0.45 μm, Sartorius) into $HgCl_2$-poisoned 10 mL glass ampoules, which were stored flame-sealed under a nitrogen atmosphere for analysis in the home laboratory. Aliquots for the determination of the remainder dissolved inorganic macronutrients were filtered through GD/X syringe filters (WHATMAN) directly into acid-washed 20 mL plastic scintillation vials and were stored frozen (−20°C) until analysis in the home laboratory. Complete ice cores were collected within 20–50 m distance from the sackhole-cored patch of the sea ice and were immediately sawed into 10 cm segments straight into plastic containers for further processing in the onboard laboratory after refrigerated melting. The ice temperature measurements were taken in a separate companion core on site by embedding a temperature probe in holes drilled to the center of the core at regular 5–10 cm intervals. All coring was conducted with a stainless

Table 1. Definitions of Biogeochemical Parameters

Parameter	Definition
C_T	= total dissolved inorganic carbon = $[CO_2(aq)] + [HCO_3^-] + [CO_3^{2-}]$
A_T	= total alkalinity = $[HCO_3^-] + 2[CO_3^{2-}] + [B(OH)_4^-] + [H^+]–[OH^-] + \Sigma A_i$, with ΣA_i = alkalinity contribution from SRP, silicic acid, ammonium, and dissolved organic matter
SRP	soluble reactive phosphorus
NO_3^-	nitrate plus nitrite
NH_4^+	dissolved ammonium
pCO_2	partial pressure of CO_2
S	practical salinity
t	temperature (°C)
s[X]	= $(^{35}/_S)$[X] = concentration of solute X normalized to salinity of 35, with X = C_T, A_T, SRP, NO_3^-, NH_4^+
$[X]_{SSW}$	concentration of solute X in surface seawater, with X = C_T, A_T, SRP, NO_3^-, NH_4^+
$s[X]_{SSW}$	= $(^{35}/_S)[X]_{SSW}$ = concentration of solute X in surface seawater normalized to salinity of 35, with X = C_T, A_T, SRP, NO_3^-, NH_4^+
$^{V_b}/_V$	sea ice porosity, with V_b = brine volume, V = bulk sea ice volume
V_o	sample volume for total alkalinity determination
V_{HCl}	cumulative acid volume added during potentiometric determination of total alkalinity
V_2	volume of acid required to reach the second equivalence point during potentiometric determination of total alkalinity
f_{H^+}	apparent activity coefficient of proton (H^+)
N_{HCl}	acid (HCl) normality
$\Delta s[X]$	= $s[X]–s[X]_{SSW}$, with X = C_T, A_T, SRP, NO_3^-, NH_4^+
ΔC_P	total dissolved inorganic carbon change due to photosynthesis
ΔC_{ppt}	total dissolved inorganic carbon change due to $CaCO_3$ precipitation
ΔC_{degas}	total dissolved inorganic carbon change due to CO_2 degassing
ΔA_P	total alkalinity change due to photosynthesis
ΔA_{ppt}	total alkalinity change due to $CaCO_3$ precipitation
$\left(^{\partial C}/_{\partial N}\right)_P$	molar ratio of the inorganic carbon to nitrogen concentration change in solution during photosynthetic uptake of total dissolved inorganic carbon and nitrate
$\left(^{\partial A}/_{\partial c}\right)_P$	molar ratio of total alkalinity to inorganic carbon concentration change in solution during photosynthetic uptake of total dissolved inorganic carbon and nitrate
$\left(^{\partial A}/_{\partial c}\right)_{ppt}$	molar ratio of total alkalinity to inorganic carbon concentration change in solution during $CaCO_3$ mineral precipitation
f_i	= $^{\Delta C_i}/_{\Delta s[C_T]}$, with *i* = photosynthesis (P), $CaCO_3$ precipitation (ppt), CO_2 degassing (degas)
$f_{i/SSW}$	= $^{\Delta C_i}/_{s[C_T]_{SSW}}$, with *i* = photosynthesis (P), $CaCO_3$ precipitation (ppt), CO_2 degassing (degas)

steel ice corer (Kovacs, 10 cm internal diameter). Additional sampling details are given in *Papadimitriou et al.* [2007] and *Norman et al.* [2011], while physical characteristics of the ice have been reported in *Haas et al.* [2009]. The surface seawater measurements presented here were selected from oceanic water profiles at 43 stations, which were collected using 12 L NISKIN bottles on a rosette sampler deployed with a conductivity-temperature-density (CTD) probe. The selection reflects oceanic water from <100 m depth in pelagic stations and <350 m depth in continental shelf stations.

3. Methods

[7] The temperature of brines and with depth in sea ice cores was measured in situ with a calibrated K–Thermocouple probe on a HANNA Instruments thermometer (HI93530). The salinity (S) of melted bulk sea ice and brines was measured at laboratory temperature (17 to 22°C) using a portable conductivity meter (SEMAT Cond 315i/SET) with a WTW Tetracon 325 probe, following dilution with de-ionized water for brines with S > 70. The porosity of sea ice (V_b/V), expressed as the percent fraction of brine volume (V_b) per unit volume of bulk ice (V), was calculated from the measured bulk sea ice salinity and temperature using the equations in *Cox and Weeks* [1983] and in *Leppäranta and Manninen* [1988].

[8] The analyses for the major dissolved inorganic nutrients, nitrate plus nitrite [hereafter, nitrate (NO_3^-)] and soluble reactive phosphorus (SRP) were done using standard colorimetric methodology [*Grasshoff et al.*, 1983] as adapted for flow injection analysis (FIA) on a LACHAT Instruments Quick-Chem 8000 autoanalyzer [*Hales et al.*, 2004]. Dissolved ammonium (NH_4^+) was determined with the fluorimetric method of *Holmes et al.* [1999] using a HITACHI F2000 fluorescence spectrophotometer. Total alkalinity (A_T) was determined by potentiometric titration of 50 mL sample with 0.1 mol L^{-1} HCl (Titrisol, Merck, Germany) using a Metrohm system of automatic burette, pH meter, platinum temperature probe, Ag/AgCl/KCl reference electrode, and glass electrode calibrated daily with NBS standards. Based on the Gran function, $F_2 = (V_o + V_{HCl})\ 10^{-pH_{NBS}} = f_{H^+}(V_2 + V_{HCl})\ N_{HCl}$, linear regression of F_2 against V_{HCl} within pH ≈ 3.9 to 3.0 (>15 data points) yields V_2 from the intercept and $A_T = V_2 \frac{N_{HCl}}{V_o}$, with V_o = sample volume, V_{HCl} = volume of added acid, f_{H^+} = apparent activity coefficient of H^+, a function of solution composition and temperature, as well as the electrode used for the measurements [*Millero*, 1995], V_2 = second equivalence point, and N_{HCl} = acid normality [*Gleitz et al.*, 1995]. Determination of A_T on CRMs (A. G. Dickson, Scripps Institution of Oceanography) yielded 2315.20 ± 0.99 μmol kg^{-1} for Batch #74 (n = 3, certified A_T = 2305.34 ± 0.68 μmol kg^{-1}, S = 34.739) and 2221.35 ± 3.13 μmol kg^{-1} for Batch #75 (n = 3, certified A_T = 2210.09 ± 0.68 μmol kg^{-1}, S = 33.228). The C_T concentration was determined following in vacuo reaction with 85% H_3PO_4 and cryogenic CO_2 gas distillation, using

Table 2. The Composition of the Surface Oceanic Water in the Western Weddell Sea[a]

Season	S	t (°C)	C_T	A_T	SRP	NO_3^-	NH_4^+
Summer[b]	34.25 ± 0.05	−0.73 ± 0.11	2193 ± 4				
Summer[c]	34.30		2149	2327	1.75	26.0	
Autumn			2191 ± 7[d]		1.90 ± 0.05[e]		
Autumn[c]	34.00	−1.80	2156	2313	1.95	29.0	1.45
Winter[b]	34.40	−1.86	2205 ± 1		1.92 ± 0.05[e]		
Spring[f]	34.40 ± 0.13 n = 103	−1.78 ± 0.14 n = 103	2224 ± 8 n = 8	2329 ± 10 n = 10	2.07 ± 0.05 n = 101	29.7 ± 0.7 n = 100	<0.05

[a]Concentrations are given as means ± 1σ (when available) in μmol kg^{-1}.
[b]July 1992 (winter), January 1993 (summer) [*Hoppema et al.*, 1995].
[c]January 1991 (summer), April 1992 (autumn) [*Gleitz et al.*, 1995].
[d]April 1996 [*Hoppema et al.*, 1999].
[e]April 1998 [*Hoppema et al.*, 2002].
[f]September–October 2006 (this study).

an in-line manometer (CHELL). Analysis of CRM (Batch #87, certified C_T = 2012.01 ± 0.62 μmol kg^{-1}, S = 33.191) yielded C_T = 2008.69 ± 3.29 μmol kg^{-1} (n = 17).

[9] All concentrations are reported on a per $kg_{solution}$ basis. While C_T was determined on a per unit weight basis, all other measurements were done on a per unit volume basis and were converted using the density of the sample at the temperature of analysis. The density was calculated by extrapolation of the equation of state for seawater in *Millero and Poisson* [1981] to the sample salinity, because the major ionic composition of sea ice-derived solutions reflects physical modification of that of oceanic water.

[10] Salts and gases dissolved in seawater are affected by physical concentration in the residual brine formed during seawater freezing. The physical concentration effect is reflected in the salinity of the brine and was eliminated by normalizing all concentration measurements to S = 35, thus uncovering any potential deviations of the concentrations in the brine from the surface seawater composition by processes other than its physical modification during seawater freezing. Linear regression was based on the Geometric Mean Regression theory [*Ricker*, 1973]. All parameters used in this study are defined in Table 1.

4. Results

4.1. Surface Seawater

[11] The salinity and temperature of the surface oceanic water during the study ranged from 34.02 to 34.58 and from −1.89 to −1.11°C, respectively. The measurements of the composition of surface seawater during the study are summarized in Table 2. Considering equivalent measurements in different seasons (Table 2), it is evident that the composition of the surface seawater in the western Weddell Sea exhibits invariable A_T but variation in the concentration of the major macronutrients, with a decrease in the summer to autumn period and an increase in late winter as a result of biological activity, air-sea exchange, sea ice melting, and transport across the pycnocline of nutrient-rich Warm Deep Water (WDW) [*Hoppema et al.*, 1995, 1999]. The surface seawater composition is required to assess the changes in the chemical composition of the brines formed during sea ice formation. The precise location and time of formation of a sea ice floe are not known, but the compositional variability in surface oceanic water from autumn through to early spring (Table 2) is small compared to the geochemical changes in the sea ice brines outlined below. Hence, the contemporaneous composition of surface seawater was used as a reference point in subsequent analysis, with the following mean (±1σ) salinity-normalized composition of nutrients and A_T: $s[NO_3^-]_{SSW}$ = 30.2 ± 0.7 μmol kg^{-1}, $s[SRP]_{SSW}$ = 2.11 ± 0.04 μmol kg^{-1}, $s[C_T]_{SSW}$ = 2264 ± 10 μmol kg^{-1}, and $s[A_T]_{SSW}$ = 2369 ± 10 μmol kg^{-1} (*see* Table 1 for detailed definitions).

4.2. Bulk Ice

[12] The ice thickness ranged from 88 cm (sackhole depth range at the site: 24 to 46 cm) to 190 cm (sackhole depth range: 25 to 64 cm). The chlorophyll maxima [*Meiners et al.*, 2009; *Norman et al.*, 2011] were observed in the lowermost 10 cm section of the ice in all cases except on 2 occasions, when the chlorophyll maximum was located in the uppermost part of the ice, and on 1 occasion, when it was located internally approximately at mid-point in an 101-cm-thick ice floe. The bulk ice temperature ranged from −8.8°C to −1.8°C, with the lowest values recorded in the upper 40 to 50 cm of the ice on most occasions, and the maximum values always in the lowermost 5 to 10 cm near the ice-seawater interface (Figures 2a–2d). The exceptions to this linear temperature increase from the uppermost to the lowest ice surfaces were the C-shaped profiles collected on 30 September 2006, 5 October 2006, and 13 October 2006 (Figures 2b and 2c). The mean (±1σ) bulk ice temperature at each ice station ranged from −2.2 ± 0.3°C to −5.3 ± 1.8°C. The bulk ice salinity ranged from 0.4 to 14.1, exhibiting mostly C-shaped profiles with depth in the ice, except for the profiles obtained at the initial ice stations (Figure 2e), which had salinity peaks at various depths in the ice column, indicating a complex thermal and growth history in these ice floes. The mean (±1σ) bulk ice salinity at each ice station ranged from 2.9 ± 1.3 to 6.9 ± 1.6. Neither the temperature nor the salinity profiles showed a discernible spatial or temporal trend.

[13] The ice porosity ranged from 0.2% to 25.7%, with a depth distribution in the ice column similar to that of bulk ice salinity (Figures 2i–2l). The mean (±1σ) ice porosity ranged from 3.5 ± 2.0% in the coldest ice cores collected on 19 September 2006 to 11.0 ± 5.6% in the warmest ice cores collected on 24 September 2006. Small-scale connectivity between pores and channels in sea ice is established at ice porosities above 5 to 7% [*Cox and Weeks*, 1975; *Golden et al.*, 1998; *Pringle et al.*, 2006]. On this basis, the coldest upper part of the ice was impermeable in the majority of the ice stations. The ice was permeable throughout its depth on few

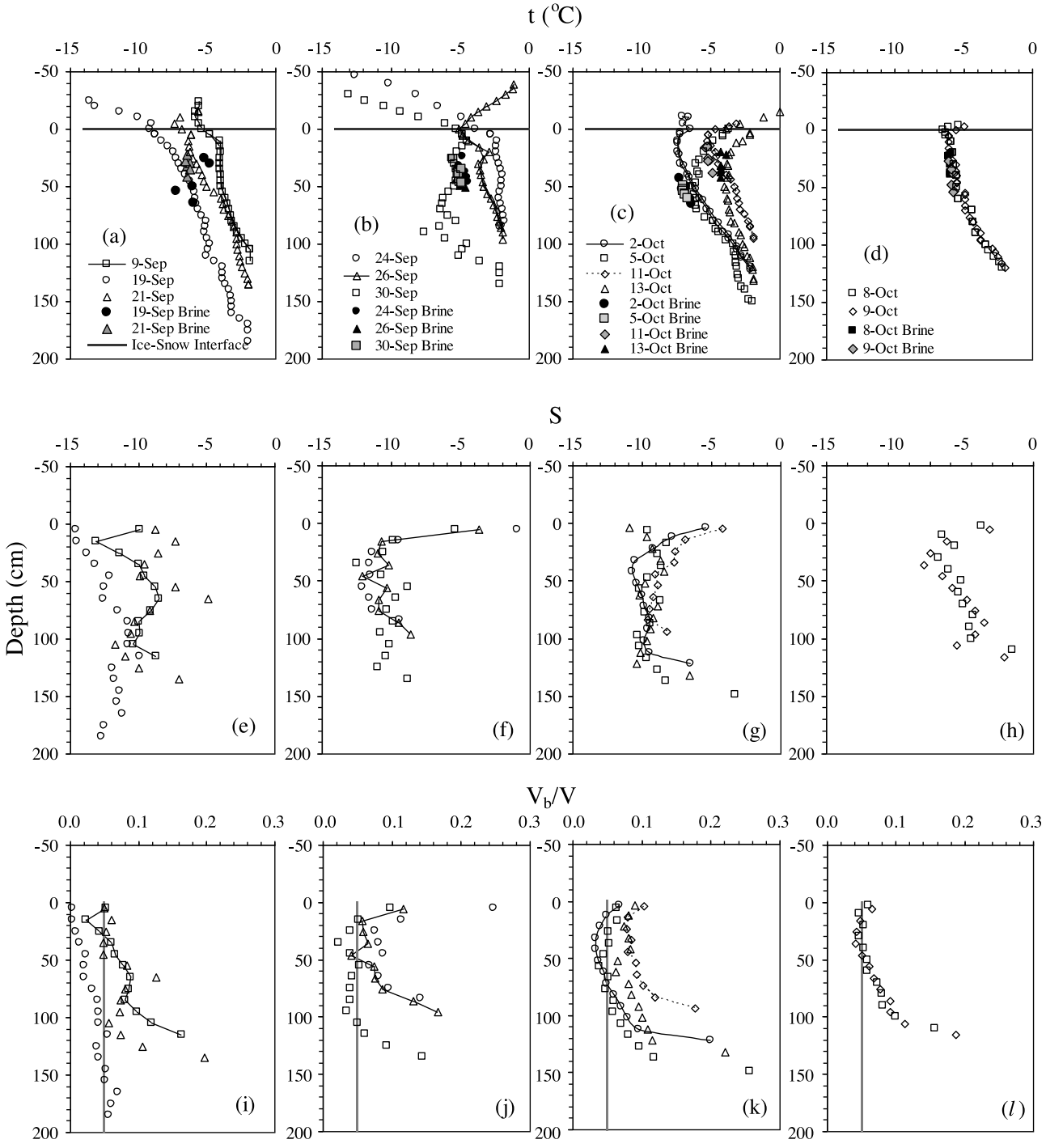

Figure 2. (a–d) Temperature, (e–h) salinity, and (i–l) relative brine volume (porosity) of bulk sea ice. The horizontal line in Figures 2a–2d indicates the ice – snow interface, with ice temperature measurements plotted on the positive depth axis and snow temperature measurements plotted on the negative depth axis. The vertical line in Figures 2i–2l represents the threshold porosity of 5% from impermeable to permeable sea ice.

occasions (24 September 2006, 11 October 2006, 13 October 2006; Figures 2j and 2k), and impermeable throughout its depth only once (19 September 2006; Figure 2i).

4.3. Brine

[14] The sackhole depths ranged from 15 to 66 cm from the ice-snow interface. The salinity (range: 58 to 134, n = 126) and temperature (range: −3.6 to −8.7°C, n = 126) of the brines have been presented and discussed in *Norman et al.* [2011]. Comparison of sackhole brine temperature with the independently measured distribution of temperature with depth in the ice (Figures 2a–2d) suggests that the brines should have originated in the coldest upper half of the ice floes, where the impermeable ice layers were located (Figures 2i–2l).

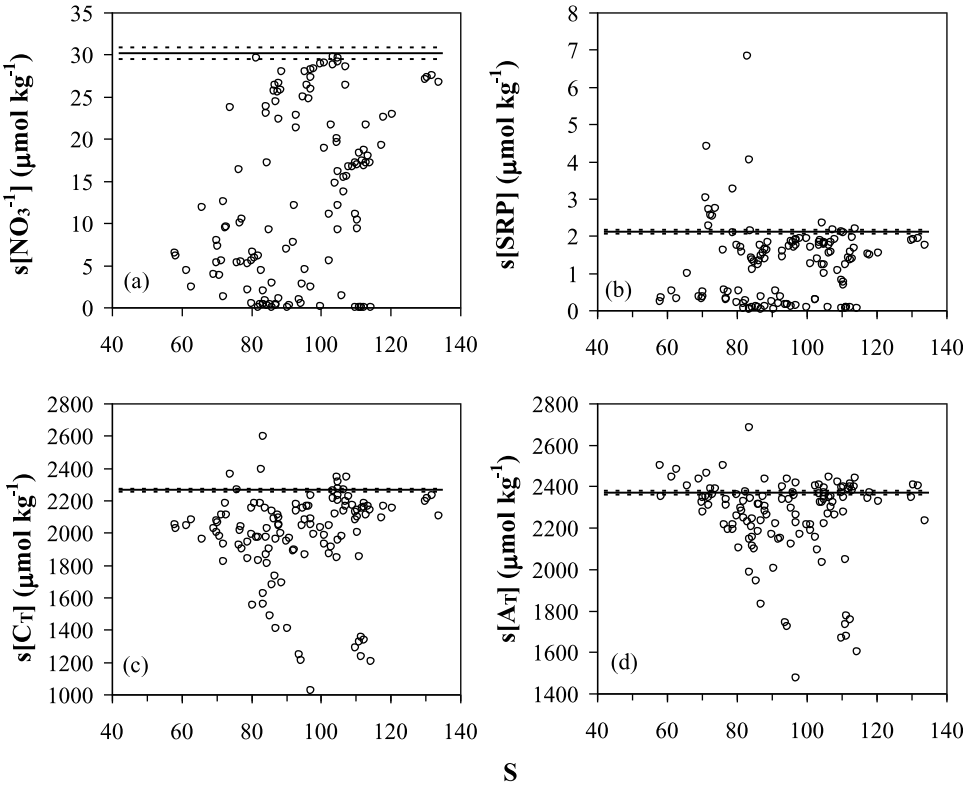

Figure 3. (a) Salinity-normalized nitrate, (b) soluble reactive phosphorus, (c) total dissolved inorganic carbon, and (d) total alkalinity versus salinity in sea ice brines. The solid line indicates the mean surface oceanic water concentration, with dashed lines indicating $\pm 1\sigma$.

[15] The measured NO_3^- concentrations ranged from 0.0 to 103.9 μmol kg^{-1} (n = 126). The salinity-normalized concentrations (s[NO_3^-]) ranged from 0.0 to 29.7 μmol kg^{-1} and show, in their vast majority, a variable deficit and no excess of NO_3^- in the brines relative to s[NO_3^-]$_{SSW}$ (Figure 3a). The measured SRP concentrations ranged from 0.07 to 16.18 μmol kg^{-1} (n = 126). The majority of the salinity-normalized concentrations (s[SRP]) also show considerable SRP deficit in the brines relative to s[SRP]$_{SSW}$ (Figure 3b). A few s[SRP] observations (range: 2.09 to 2.16 μmol kg^{-1}, n = 5) were close to s[SRP]$_{SSW}$ within its uncertainty or were considerably higher than s[SRP]$_{SSW}$, indicating relative SRP enrichment in the brine (range: 2.20 to 6.82 μmol kg^{-1}, n = 12) (Figure 3b). The measured NH_4^+ concentrations ranged from <0.05 to 35.59 μmol kg^{-1} (n = 123). The salinity-normalized concentrations (s[NH_4^+]) ranged from <0.05 to 11.59 μmol kg^{-1}, being mostly higher than s[NH_4^+]$_{SSW}$. This almost ubiquitous relative NH_4^+ enrichment in the brines was modest in most cases, with a mean ($\pm 1\sigma$) s[NH_4^+] = 0.30 $\pm$ 0.19 μmol kg^{-1} (n = 102), but a few s[NH_4^+] observations exceeded 1 μmol kg^{-1}, with a mean ($\pm 1\sigma$) s[NH_4^+] = 5.64 $\pm$ 3.55 μmol kg^{-1}, n = 21 (Figure 4d).

[16] The measured C_T ranged from 2839 to 8405 μmol kg^{-1} (n = 123). Only a small number (n = 4) of the salinity-normalized observations (s[C_T]) were close (within variability as $\pm 1\sigma$) to the average s[C_T]$_{SSW}$ (Figure 3c). Also few observations indicated relative C_T excess, with a mean ($\pm 1\sigma$) Δs[C_T] = s[C_T]–s[C_T]$_{SSW}$ = 129 $\pm$ 103 μmol kg^{-1} (range: 48 to 333 μmol kg^{-1}, n = 6). On most occasions, the salinity-normalized C_T observations indicated a relative deficit, ranging from −32 to −1239 μmol kg^{-1}, with a mean ($\pm 1\sigma$) Δs[C_T] = −314 $\pm$ 270 μmol kg^{-1} (n = 113). The measured A_T ranged from 3912 to 9054 μmol kg^{-1} (n = 121). A small number of salinity-normalized observations (s[A_T]) were close to s[A_T]$_{SSW}$ (Figure 3d) within the variability of this concentration and the uncertainty of the titrations, with a mean ($\pm 1\sigma$) Δs[A_T] = s[A_T]–s[A_T]$_{SSW}$ = −2 $\pm$ 6 μmol kg^{-1} (range: 7 to −12 μmol kg^{-1}, n = 9). A few observations with a mean ($\pm 1\sigma$) Δs[A_T] = 61 $\pm$ 60 μmol kg^{-1} indicated relative excess of A_T (range: 16 to 315 μmol kg^{-1}, n = 28). In the majority of the samples, the salinity-normalized concentrations yielded a relative deficit, with a mean ($\pm 1\sigma$) Δs[A_T] = −192 $\pm$ 203 μmol kg^{-1} (range: −893 to −16 μmol kg^{-1}, n = 84).

5. Discussion

5.1. Dissolved Inorganic Carbon Sinks in Sea Ice

[17] The mass balance of total dissolved inorganic carbon in sea ice brine is controlled by photosynthetic production of microorganisms, by respiration of all sea ice biota, by $CaCO_3$ mineral precipitation and dissolution, and by CO_2 degassing and uptake. Photosynthesis, $CaCO_3$ precipitation, and CO_2 degassing lead to a C_T concentration deficit relative to the C_T concentration in the surface oceanic water at the time of brine formation during seawater freezing, while respiration, $CaCO_3$ dissolution, and CO_2 uptake cycle carbon back into the C_T pool from the organic, mineral, and gaseous phases, respectively. The observed s[C_T] is the result of a combination of some or all the above processes, leading to either a net deficit or excess relative concentration in the evolving sea ice

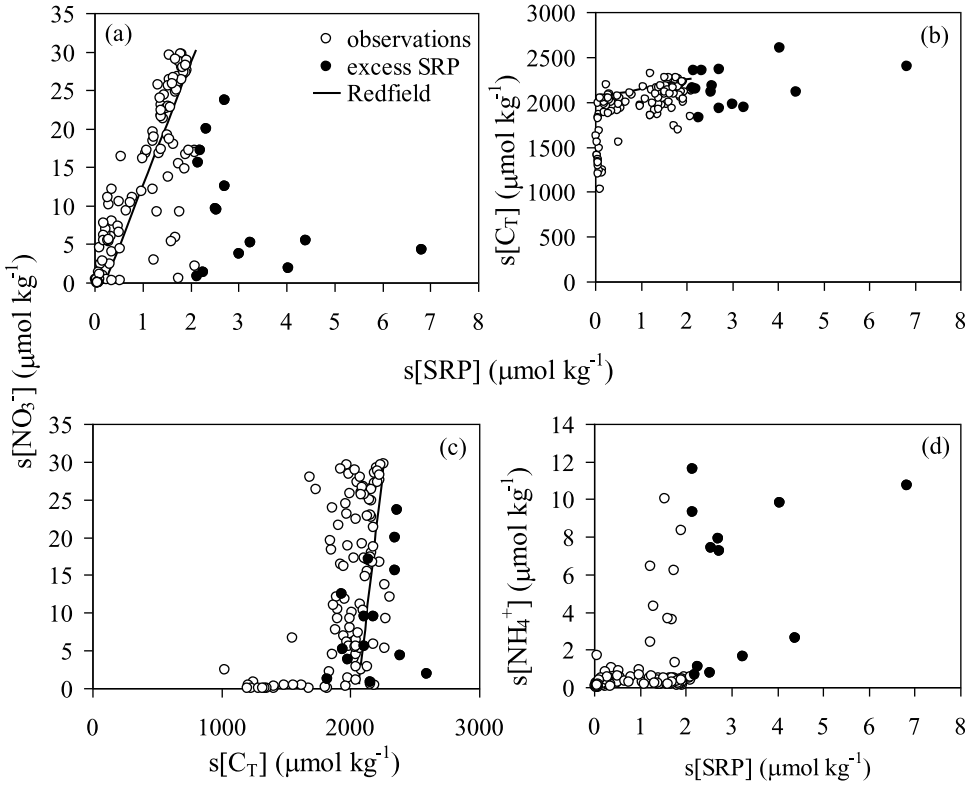

Figure 4. Dissolved inorganic macro-nutrient pairs in sea ice brines (concentrations normalized to salinity of 35). Open symbols represent observations with $s[SRP] \leq s[SRP]_{SSW}$, while closed symbols represent observations with $s[SRP] > s[SRP]_{SSW}$. The straight line in Figures 4a, 4b, and 4c indicates concentration changes at a molar ratio equivalent to the Redfield stoichiometry (C:N:P = 106:16:1).

brine. The observations were obtained during the transition from winter to spring over a large geographical expanse in the Weddell Sea, a rare opportunity in terms of space and time for sea ice studies. The ice temperature, salinity, and V_b/V profiles (Figure 2) also illustrate this transition from the cold and impermeable ice conditions during winter to the warm and permeable conditions typical of summer sea ice [*Geilfus et al.*, 2012]. The majority of the brine samples (92%) yielded a deficit in $s[C_T]$, as was also the case in sea ice brines and surface gap layers in late austral spring and early austral summer [*Papadimitriou et al.*, 2007, 2009; *Munro et al.*, 2010]. The maximum deficit observed here was equivalent to 55% of $s[C_T]_{SSW}$. The observations indicate that the C_T-consuming processes dominated the concentration changes seen during the winter to spring transition. On these occasions, therefore, the mass balance for the observed deficit in $s[C_T]$, $\Delta s[C_T] = s[C_T] - s[C_T]_{SSW}$ (see Table 1 for definitions), can be formulated as the sum of the fractional deficits caused by net photosynthesis (ΔC_P), net $CaCO_3$ mineral precipitation (ΔC_{ppt}), and degassing of the dissolved CO_2 in the brine (ΔC_{degas}), i. e., $\Delta s[C_T] = \Delta C_P + \Delta C_{ppt} + \Delta C_{degas}$. To quantify the fractional contribution of each of the processes to the inorganic carbon cycle in sea ice, each fractional deficit is derived in the subsequent sections using the observed s[SRP], $s[NO_3^-]$, and $s[A_T]$ deviations from conservative behavior during seawater freezing.

5.1.1. Biological Activity

[18] The observed deviations of $s[NO_3^-]$ and s[SRP] in the brines from the concentration in surface oceanic water comprise the imprint of biological activity [*Gleitz et al.*, 1995; *Papadimitriou et al.*, 2007]. On most occasions, the brines were deficient in these macro-nutrients and $s[C_T]$, with co-dependent concentration changes forming a central trend with a linear slope similar to the Redfield stoichiometry for inorganic nutrient uptake during photosynthesis, based on the major element quota of pelagic phytoplankton (C:N:P = 106:16:1 [*Redfield et al.*, 1963]) (Figure 4). The effect of autotrophic activity on the chemical composition of sea ice has been commonly observed in studies of sea ice habitats conducted from early summer to early autumn, where active sympagic micro-algal communities are common [*Fritsen et al.*, 1994; *Gleitz et al.*, 1995; *Kennedy et al.*, 2002; *Papadimitriou et al.*, 2007, 2009]. However, the closeness of the chemical changes to the Redfield stoichiometry observed here was not evident in sea ice brine studies later in summer [*Gleitz et al.*, 1995; *Papadimitriou et al.*, 2007]. In this study, the imprint of autotrophic activity was derived from the upper part of the ice column, away from the concurrent chlorophyll (as a proxy for autotrophic biomass) maximum. Moreover, photosynthetic parameters measured by Pulse Amplitude Modulation (PAM) fluorometry in selected ice stations suggested moderate autotrophic activity in bottom and internal sympagic micro-algal communities at the time of the study [*Meiners et al.*, 2009]. In light of this, it is conceivable that, at least, part of the photosynthetic imprint on the major dissolved inorganic nutrient concentrations in the brines discussed here was a relic of an autumn bloom when and where the sea ice had formed.

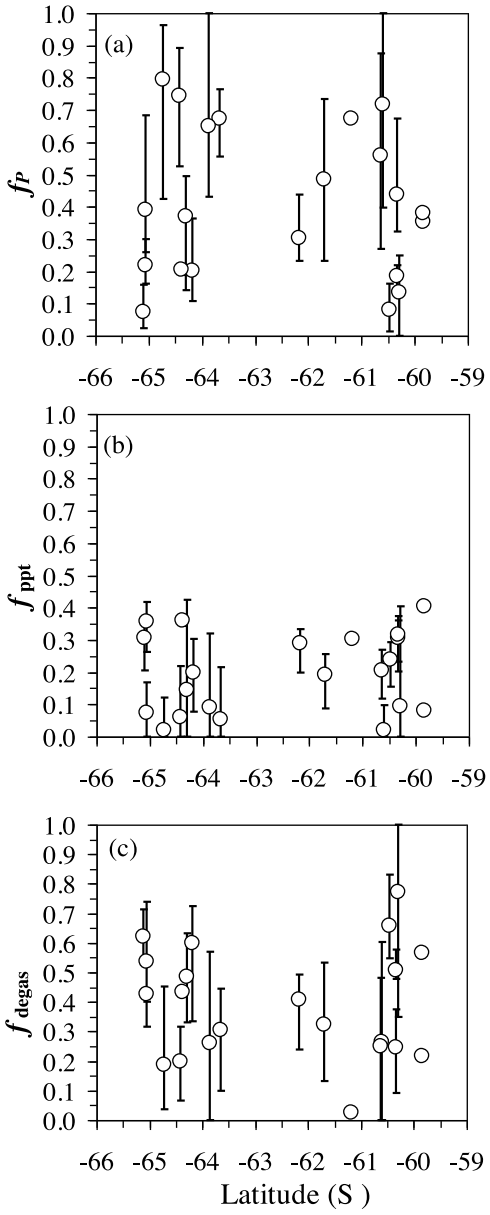

Figure 5. Fractional deficits relative to the total deficit of total dissolved inorganic carbon due to (a) photosynthesis, (b) $CaCO_3$ precipitation, and (c) CO_2 degassing versus latitude. Circles indicate mean values and error bars indicate the range of values at each ice station.

[19] On the few occasions when s[SRP] enrichment was observed in the brines relative to the surface oceanic water, there was also relative enrichment in the s[C_T] and s[NH_4^+] concentrations in the brine but not in the s[NO_3^-] concentration (Figure 4). On these occasions, the observed accumulation of dissolved inorganic metabolites in the brine in excess of their surface seawater concentrations suggests remineralization via utilization of particulate and dissolved organic substrates that had become trapped in the ice prior to brine channel isolation. Moreover, it appears that, in those cases, organic nitrogen metabolism resulted in ammonium regeneration (ammonification) rather than NO_3^- regeneration via nitrification of the regenerated NH_4^+.

[20] The fractional contribution of photosynthesis to the observed s[C_T] deficit is defined as

$$f_P = \Delta C_p \Big/ \Delta s[C_T], \quad (1)$$

The f_P can be calculated from the NO_3^- deficit because $\Delta C_P = \left(\partial C/\partial N\right)_P \Delta s[NO_3^-]$, provided that the stoichiometry of the biological reaction $\left(\partial C/\partial N\right)_P$ is constant in space and time, and is known. The plots of nutrient pairs (Figure 4) indicated that the stoichiometry of the biological reaction in these sea ice brines was close to the Redfield C:N:P stoichiometry of 106:16:1 [*Redfield et al.*, 1963], which was adopted as an approximation for the calculations. The same equation can be written for the calculation of ΔC_P from the s[SRP] deficit. The f_P estimates from both s[SRP] and s[NO_3^-], f_P^{SRP} and $f_P^{NO_3^-}$, respectively, differed from each other in each brine sample. The mean ($\pm 1\sigma$) difference in the majority of the samples ($n = 89$) was $f_P^{SRP} - f_P^{NO_3^-} = 0.06 \pm 0.09$, implying an uncertainty of up to 15% in this type of calculation. Large discrepancies between f_P^{SRP} and $f_P^{NO_3^-}$ were calculated on several occasions ($n = 34$) when a deficit in s[NO_3^-] was coupled with excess or minimal deviation of s[SRP] and s[C_T] from the surface seawater concentrations. The decoupling of the nutrient cycling implicit in these latter observations suggests that NO_3^- may be less affected than SRP by remineralization and should thus be a more reliable indicator of net photosynthetic activity on these occasions, and it is adopted as such in this study. Thus, the NO_3^--based f_P is used hereafter, which ranged from 0.00 to 1.00 (Figure 5a), with a mean ($\pm 1\sigma$) of 0.41 ± 0.27 ($n = 107$). The $f_P^{NO_3^-}$ range indicates that (net) photosynthetic activity can drive up to 100% of the observed sC_T deficit in the brine.

[21] The $\Delta s[C_T]$ was variable; using it as, effectively, a normalizing factor of the also variable fractional deficits in the mass balance calculations for C_T (equation (1)) illustrates the relative strength of each inorganic carbon-consuming process on each occasion. To compare the magnitude of the fractional deficits across all available samples, the salinity-normalized concentration of C_T in surface seawater is used as a constant and common denominator. Hence, expressing the calculated ΔC_P as a fraction of $s[C_T]_{SSW}$ yielded $f_{P/SSW} = \Delta C_p / s[C_T]_{SSW} = 0.00$–$0.09$. The $f_{P/SSW}$ range indicates that, although photosynthesis can be responsible for up to 100% of the C_T deficit in individual sea ice brines (i.e., $f_P = 1.00$), this photosynthetic deficit will not exceed an upper limit equivalent to 9% of the surface oceanic C_T concentration (i.e., $f_{P/SSW} = 0.09$), corresponding to the occasions when brines were depleted of NO_3^-. This maximum value is therefore imposed by nutrient availability, which can be limiting in a porous medium with seasonally restricted capacity for replenishment of solutes by exchange with surface seawater.

5.1.2. Carbonate Mineral Precipitation and CO_2 Degassing

[22] The total alkalinity in the oceans is mostly controlled by the formation-dissolution cycle of $CaCO_3$ minerals, and one of the diagnostic stoichiometric relationships is that between the A_T and C_T in solutions which are in contact with $CaCO_3$. The process in circum-neutral pH conditions is

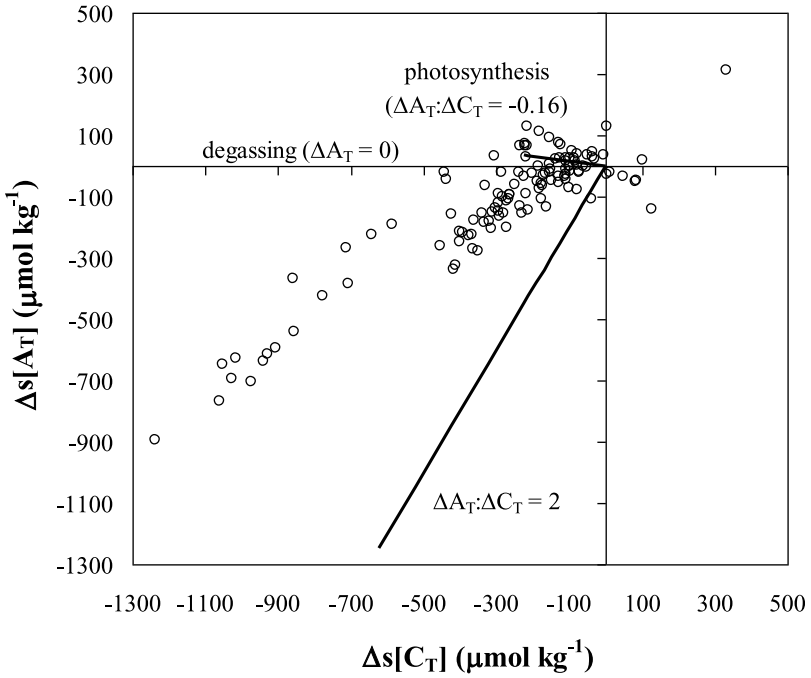

Figure 6. Change in the concentration of salinity-normalized total alkalinity as a function of the change in the concentration of salinity-normalized total dissolved inorganic carbon in sea ice brines.

described by the equilibrium reaction, $Ca^{2+} + 2\ HCO_3^- \leftrightarrow CaCO_3 + CO_2 + H_2O$, with concurrent decrease in the concentration of A_T and C_T during precipitation, and vice versa during dissolution, at a molar ratio, $\Delta A_T:\Delta C_T = 2$. Biological activity has, in comparison, an almost negligible effect on A_T, primarily via nitrate cycling, with $\Delta A_T:\Delta C_T = -0.16$ [*Lazar and Loya*, 1991].When CO_2 degassing is the sole process affecting the CO_2 system, then $\Delta A_T = 0$.

[23] The current observations include $s[A_T]$ deficits on several occasions (Figure 3d), which co-vary with the $s[C_T]$ deficits along a central trend with a positive slope of 0.7 ± 0.1 (r_{linear} = 0.911, n = 120), implying the presence of $CaCO_3$ mineral phase(s) in the brines (Figure 6). The shift of this trend from a solely $CaCO_3$-influenced ΔA_T to ΔC_T molar ratio of 2 toward both $\Delta A_T = 0$ and the barely discernible trend with a slope equivalent to a $\Delta A_T:\Delta C_T = -0.16$ can be understood as the varying influence of CO_2 degassing and photosynthesis, respectively. A similar trend was observed also in late winter and spring at several ice stations in the Beaufort Sea in the Arctic region, leading to an analogous conclusion [*Geilfus et al.*, 2012].

[24] Based on the above, it appears that $CaCO_3$ formation had some influence on the CO_2 system in the sea ice brines studied here. Ikaite ($CaCO_3 \cdot 6H_2O$) was identified as the mineral product of this process at various depths in sea ice in companion cores at some of the ice stations by *Dieckmann et al.* [2008]. The exact brine composition where the mineral was found is not known, but the adjacent sackholes yielded brine with A_T and C_T deficits distributed throughout the observed range of deficits in these parameters. This mineral phase is predicted to begin to precipitate at −5°C in sea ice brines at equilibrium with a pCO_2 = 364 μatm [*Marion*, 2001], with an inverse relationship between the temperature of onset of precipitation and brine pCO_2 [*Papadimitriou et al.*, 2007]. Specifically, as the degree of saturation of a solution with respect to $CaCO_3$ minerals is a function of the concentration of CO_3^{2-} and, by extension, of the pH and pCO_2 of the solution, the temperature field of ikaite precipitation and stability in sea ice brines can extend well above the −5.0°C threshold in low pCO_2 (i.e., alkaline pH) conditions. This situation will be aided by biological inorganic carbon uptake, which can drive the pCO_2 of sea ice brines to as low as 100 μatm or lower [*Delille et al.*, 2007; *Papadimitriou et al.*, 2007]. This is consistent with the systematic photosynthetic effect evident from the dissolved inorganic macro-nutrients (Figure 4).

[25] The fractional contribution of $CaCO_3$ mineral precipitation to the $s[C_T]$ deficit is defined as $f_{ppt} = \Delta C_{ppt} \Big/ \Delta s[C_T]$. The f_{ppt} is calculated from the mass balance for $\Delta s[A_T]$, $\Delta s[A_T] = \Delta A_P + \Delta A_{ppt}$, by relating the change in total alkalinity due to photosynthesis (ΔA_P) and $CaCO_3$ precipitation (ΔA_{ppt}) to ΔC_P and ΔC_{ppt}, respectively, via their molar stoichiometric ratios in a closed system. Given that $\Delta C_P = f_P \Delta s[C_T]$ and $\Delta C_{ppt} = f_{ppt} \Delta s[C_T]$, re-writing the mass balance equation for $\Delta s[A_T]$ above as a function of $\Delta s[C_T]$ and then solving for f_{ppt} leads to

$$f_{ppt} = \left[\left(\frac{\Delta s[A_T]}{\Delta s[C_T]} \right) - f_P \left(\frac{\partial a}{\partial C} \right)_P \right] \Bigg/ \left(\frac{\partial A}{\partial C} \right)_{ppt}, \qquad (2)$$

with $f_P = NO_3^-$-based fractional contribution of photosynthesis to $\Delta s[C_T]$ outlined earlier, $\left(\partial A/\partial c\right)_P = -0.16$ = stoichiometry of photosynthesis, and $\left(\partial A/\partial c\right)_{ppt} = 2$ = stoichiometry of $CaCO_3$ precipitation. These calculations yielded a range of

f_{ppt} between 0.00 and 0.42 (Figure 5b) with a mean ($\pm 1\sigma$) of 0.18 ± 0.14 (n = 102), indicating an upper limit for the net fractional C_T deficit via $CaCO_3$ precipitation, equivalent to 42% of $\Delta s[C_T]$. The $f_{ppt/SSW}$ range from 0.00 to 0.20 indicates that net $CaCO_3$ precipitation can result in the removal of a maximum amount of C_T from the sea ice brines equivalent to 20% of $s[C_T]_{SSW}$.

[26] Following the determination of f_P and f_{ppt} above, the fractional contribution of CO_2 degassing to $\Delta s[C_T]$ can be calculated as $f_{degas} = 1 - f_P - f_{ppt}$, yielding a range from 0.00 to 1.00 (Figure 5c), with a mean ($\pm 1\sigma$) of 0.41 ± 0.22 (n = 102). Similarly to f_P, CO_2 degassing appears to have driven up to 100% of the $s[C_T]$ deficit in the brines on occasion, and was responsible for the removal of a maximum amount of C_T from the sea ice brines equivalent to 26% of $s[C_T]_{SSW}$ (i.e., $f_{degas/SSW}$ range from 0.00 to 0.26).

[27] This analysis shows that either net photosynthetic activity or CO_2 degassing dominated C_T-consumption in sea ice brines by driving more than 50% of the observed $s[C_T]$ deficits on several occasions, while net $CaCO_3$ precipitation always accounted for less than 50% of $\Delta s[C_T]$ (Figure 5). However, viewed relative to the stable parameter of $s[C_T]_{SSW}$, the largest deficits were always associated with $CaCO_3$ precipitation and CO_2 degassing, because the magnitude of the photosynthetic C_T deficit is limited by the size of the inorganic nutrient pool. In other words, $s[C_T]$ deficits in excess of 200 to 300 μmol kg^{-1} could only have been driven by CO_2 degassing and $CaCO_3$ precipitation. The inorganic carbon deficits exhibited large spatial variability, even within 1 m^2 of an ice floe, and there was no discernible geographical pattern (Figure 5). Further, there was no relationship with brine temperature, a key variable in CO_2 degassing and $CaCO_3$ precipitation, controlling gaseous and mineral equilibria along with salinity [*Marion*, 2001; *Papadimitriou et al.*, 2004]. This, however, is not altogether unexpected in opportunistic sampling, with the averaging out of properties in bulk samples.

5.2. Implications for the CO_2 Flux in Sea Ice-Covered Oceans

[28] The role of biological production in the carbon budget of ice-covered oceans has held the attention of polar scientists for several decades. Photosynthetic activity requires light, nutrients, and the warmer end of the temperature spectrum in sea ice. It decreases dramatically the dissolved CO_2 in the sea ice aqueous habitats [*Kennedy et al.*, 2002; *Delille et al.*, 2007; *Papadimitriou et al.*, 2007, 2009] and thus generates a negative pCO_2 gradient from the atmosphere toward the sea ice, potentially leading to a pCO_2 invasion, sea ice permeability allowing [*Geilfus et al.*, 2012].

[29] In comparison, CO_2 degassing and the $CaCO_3$ mineral cycle, although endemic in natural sea ice, are poorly documented. The effect of these abiotic processes on the air-sea CO_2 cycling in the sea-ice-covered polar regions will depend on whether the dissolved inorganic carbon deficits, which they cause, result in transport across the sea ice column through the microscopic brine channel system toward the ice-seawater and the ice-air interfaces. The timing of the dissolved inorganic carbon loss via these processes within the physics of the sea ice formation–decay cycle is crucial in this respect. The following reasoning is offered as an example along these lines.

[30] The sampled brines originated in the upper ice layers, which were impermeable at the time of sampling in most ice stations (Figures 2i–2l) and even more so in the previous winter months at colder temperatures and lower ice permeability. This suggests that the brines had been isolated, representing a closed system, for some period in their thermal history after sea ice consolidation. If the $s[C_T]$ deficits connected with CO_2 degassing and $CaCO_3$ precipitation occurred solely during the period of cold temperatures and minimum ice permeability, when the brine channels were isolated from the ocean and the atmosphere, they should reduce in magnitude during the decay phase of sea ice via warming up and melting by the reverse processes of respiration, CO_2 solution, and $CaCO_3$ dissolution. In this way, the effect of the abiotic C_T consumption on air-sea exchange during the period of increasing connectivity across the ocean–ice–air system later in the warming spring-summer season will lessen. In short, a deficit in C_T in sea ice is a transient feature; its magnitude in cold brines in the impermeable upper parts of sea ice may not translate in an instantaneous or steady state carbon transport through the sea ice column along a chemical gradient.

[31] The effect of $CaCO_3$ mineral dynamics will thus depend on whether their precipitation-dissolution cycle in sea ice is closed, beginning and ending in the brine channels. The degassing of brine CO_2, however, has two distinctive components during the formation and consolidation stages of sea ice. One component occurs during the early stages of sea ice formation and growth at maximum connectivity with the atmosphere and the ocean, as seen experimentally [*Killawee et al.*, 1998; *Papadimitriou et al.*, 2004]. The inorganic carbon lost to gas bubbles at the ice-seawater interface at this initial stage of sea ice formation will be viable to exchange with the atmosphere. This loss will be associated with gross sea ice production and will be further modulated by the hydrodynamics near the ice-seawater interface [*Killawee et al.*, 1998; *Loose et al.*, 2009], resulting in CO_2 evasion, as observed in leads and polynyas [*Else et al.*, 2011]. The second component of CO_2 degassing will be associated with the disequilibrium, as CO_2 supersaturation, generated by physical concentration and $CaCO_3$ mineral precipitation in the internal brines during the growth and consolidation stage of sea ice. The CO_2 thus lost to internal gas bubbles will give rise to an internal CO_2 gradient, which can facilitate air-sea exchange through sea ice [*Loose et al.*, 2011b].

[32] The current observations show that the sea ice cover is a potent carbon reactor. All three major oceanic carbon cycling processes, i.e., biological productivity, $CaCO_3$ mineral reactions, and CO_2 gas exchange, occur in the elaborate, physically and chemically dynamic brine channel system of sea ice. The associated net concentration deficits of dissolved inorganic carbon can support CO_2 fluxes among the sea, the sea ice, and the atmosphere, which are beginning to be documented in the sea-ice covered seas [*Else et al.*, 2011; *Miller et al.*, 2011; *Geilfus et al.*, 2012]. This and the sizable polar-ocean-wide budget in the peta-gram range from the tentative and conservative scaling-up of similar calculations in *Munro et al.* [2010] makes the elucidation of these processes in sea ice clearly worth pursuing.

[33] **Acknowledgments.** We are grateful to the crew of *R. V. Polarstern* who made the work possible. We thank Christian Haas and Marcel Nicolaus for

their help in the field and for supplying ice core temperature data. We also thank E. Allhusen for her help in preparation for the cruise, and for sample collection and analyses during the cruise. The work was supported by grants from NERC (grant NER/A/S/2003/00340), the Royal Society, and the Leverhulme Trust.

References

Anderson, L. G., E. Falck, E. P. Jones, S. Jutterström, and J. H. Swift (2004), Enhanced uptake of atmospheric CO_2 during freezing of seawater: A field study in Storfjorden, Svalbard, *J. Geophys. Res.*, *109*, C06004, doi:10.1029/2003JC002120.

Arrigo, K. R., G. van Dijken, and M. Long (2008), Coastal Southern Ocean: A strong anthropogenic CO_2 sink, *Geophys. Res. Lett.*, *35*, L21602, doi:10.1029/2008GL035624.

Cox, G. F. N., and W. F. Weeks (1975), Brine drainage and initial salt entrapment in sodium chloride ice, *CRREL Res. Rep. 345*, Cold Reg. Res. and Eng. Lab., Hanover, N. H.

Cox, G. F. N., and W. F. Weeks (1983), Equations for determining the gas and brine volumes in sea ice samples, *J. Glaciol.*, *29*, 306–316.

Delille, B., B. Jourdain, A. V. Borges, J. L. Tison, and D. Delille (2007), Biogas (CO_2, O_2, dimethylsulfide) dynamics in spring Antarctic fast ice, *Limnol. Oceanogr.*, *52*, 1367–1379, doi:10.4319/lo.2007.52.4.1367.

Dieckmann, G. S., G. Nehrke, S. Papadimitriou, J. Gottlicher, R. Steininger, H. Kennedy, D. Wolf-Gladrow, and D. N. Thomas (2008), Calcium carbonate as ikaite crystals in Antarctic sea ice, *Geophys. Res. Lett.*, *35*, L08501, doi:10.1029/2008GL033540.

Dieckmann, G. S., G. Nehrke, C. Uhlig, J. Göttlinger, S. Gerland, M. A. Granskog, and D. N. Thomas (2010), Brief communication: Ikaite ($CaCO_3 \cdot 6H_2O$)) discovered in Arctic sea ice, *Cryosphere*, *4*, 227–230, doi:10.5194/tc-4-227-2010.

Else, B. G. T., T. N. Papakyriakou, R. J. Galley, W. M. Drennan, L. A. Miller, and H. Thomas (2011), Wintertime CO_2 fluxes in an Arctic polynya using eddy covariance: Evidence for enhanced air-sea gas transfer during ice formation , *J. Geophys. Res.*, *116*, C00G03, doi:10.1029/2010JC006760.

Fritsen, C. H., V. I. Lytle, S. F. Ackley, and C. W. Sullivan (1994), Autumn bloom of Antarctic pack-ice algae, *Science*, *266*, 782–784, doi:10.1126/science.266.5186.782.

Geilfus, N. X., G. Carnat, T. N. Papakyriakou, J. L. Tison, B. Else, H. Thomas, E. Shadwick, and B. Delille (2012), Dynamics of pCO_2 and related air-ice CO_2 fluxes in the Arctic coastal zone (Amundsen Gulf, Beaufort Sea), *J. Geophys. Res.*, *117*, C00G10, doi:10.1029/2011JC007118.

Gleitz, M., M. Rutgers van der Loeff, D. N. Thomas, G. S. Dieckmann, and F. J. Millero (1995), Comparison of summer and winter inorganic carbon, oxygen and nutrient concentrations in Antarctic sea ice brines, *Mar. Chem.*, *51*, 81–91, doi:10.1016/0304-4203(95)00053-T.

Golden, K. M., S. F. Ackley, and V. I. Lytle (1998), The percolation phase transition in sea ice, *Science*, *282*, 2238–2241, doi:10.1126/science.282.5397.2238.

Grasshoff, K., M. Ehrhardt, and K. Kremling (1983), *Methods of Seawater Analysis*, Verlag Chemie, Weinheim, Germany.

Haas, C., A. Friedrich, Z. Li, M. Nicolaus, A. Pfaffling, and T. Toyota (2009), Regional variability of sea ice properties and thickness in the northwestern Weddell Sea obtained by in-situ and satellite measurements, in *Cruise Report Winter Weddell Outflow Study (WWOS)-ANT XXIII/7*, *Rep. Polar Res. 586*, pp. 36–74, Alfred Wegener Inst. for Polar and Mar. Res., Potsdam, Germany.

Hales, B., A. van Greer, and T. Takahashi (2004), High-frequency measurements of seawater chemistry: Flow-injection analysis of macronutrients, *Limnol. Oceanogr. Methods*, *2*, 91–101, doi:10.4319/lom.2004.2.91.

Holmes, R. M., A. Aminot, R. Kerouel, B. A. Hocker, and B. J. Peterson (1999), A simple and precise method for measuring ammonium in marine and fresh water, *Can. J. Fish. Aquat. Sci.*, *56*, 1801–1808, doi:10.1139/cjfas-56-10-1801.

Hoppema, M., E. Fahrbach, M. Schröder, A. Wisotzki, and H. J. W. de Baar (1995), Winter-summer differences of carbon dioxide and oxygen in the Weddell Sea surface layer, *Mar. Chem.*, *51*, 177–192, doi:10.1016/0304-4203(95)00065-8.

Hoppema, M., E. Fahrbach, M. H. C. Stoll, and H. J. W. de Baar (1999), Annual uptake of atmospheric CO_2 by the Weddell Sea derived from a surface layer balance, including estimations of entrainment and new production, *J. Mar. Syst.*, *19*, 219–233, doi:10.1016/S0924-7963(98)00091-8.

Hoppema, M., H. J. W. de Baar, R. G. J. Bellerby, E. Fahrbach, and K. Bakker (2002), Annual export production in the interior Weddell gyre estimated from a chemical mass balance of nutrients, *Deep Sea Res., Part II*, *49*, 1675–1689, doi:10.1016/S0967-0645(02)00006-1.

Jutterström, S., and L. Anderson (2010), Uptake of CO_2 by the Arctic Ocean in a changing climate, *Mar. Chem.*, *122*, 96–104, doi:10.1016/j.marchem.2010.07.002.

Kennedy, H., D. N. Thomas, G. Kattner, C. Haas, and G. S. Dieckmann (2002), Particulate organic matter in Antarctic summer sea ice: Concentration and stable isotopic composition, *Mar. Ecol. Prog. Ser.*, *238*, 1–13, doi:10.3354/meps238001.

Killawee, J. A., I. J. Fairchild, J. L. Tison, L. Janssens, and R. Lorrain (1998), Segregation of solutes and gases in experimental freezing of dilute solutions: Implications for natural glacial systems, *Geochim. Cosmochim. Acta*, *62*, 3637–3655, doi:10.1016/S0016-7037(98)00268-3.

Lazar, B., and Y. Loya (1991), Bioerosion of coral reefs—A chemical approach, *Limnol. Oceanogr.*, *36*, 377–383, doi:10.4319/lo.1991.36.2.0377.

Lemke, P. (2009), Itinerary and summary, in *Cruise Report Winter Weddell Outflow Study (WWOS)-ANT XXIII/7*, *Rep. Polar Res. 586*, pp. 10–11, Alfred Wegener Inst. for Polar and Mar. Res., Potsdam, Germany.

Leppäranta, M., and T. Manninen (1988), The brine and gas content of sea ice with attention to low salinities and high temperatures, *Internal Rep. 88-2*, Finnish Inst. of Mar. Res., Helsinki.

Loose, B., and P. Schlosser (2011), Sea ice and its effect on CO_2 flux between the atmosphere and the Southern Ocean interior, *J. Geophys. Res.*, *116*, C11019, doi:10.1029/2010JC006509.

Loose, B., W. R. McGillis, P. Schlosser, D. Perovich, and T. Takahashi (2009), Effects of freezing, growth, and ice cover on gas transport processes in laboratory seawater experiments, *Geophys. Res. Lett.*, *36*, L05603, doi:10.1029/2008GL036318.

Loose, B., L. A. Miller, S. Elliott, and T. N. Papakyriakou (2011a), Sea ice biogeochemistry and material transport across the frozen interface, *Oceanography*, *24*, 202–218, doi:10.5670/oceanog.2011.72.

Loose, B., P. Schlosser, D. Perovich, D. Ringelberg, D. T. Ho, T. Takahashi, J. Richter-Menge, C. M. Reynolds, W. R. McGillis, and J. L. Tison (2011b), Gas diffusion through columnar laboratory sea ice: Implications for mixed-layer ventilation of CO_2 in the seasonal ice zone, *Tellus, Ser. B*, *63*, 23–39, doi:10.1111/j.1600-0889.2010.00506.x.

Marion, G. M. (2001), Carbonate mineral solubility at low temperatures in the Na-K-Mg-Ca-H-Cl-SO_4-OH-HCO_3-CO_3-CO_2-H_2O system, *Geochim. Cosmochim. Acta*, *65*, 1883–1896, doi:10.1016/S0016-7037(00)00588-3.

Meiners, K. M., S. Papadimitriou, D. N. Thomas, L. Norman, and G. S. Dieckmann (2009), Biogeochemical conditions and ice algal photosynthetic parameters in Weddell Sea ice during early spring, *Polar Biol.*, *32*, 1055–1065, doi:10.1007/s00300-009-0605-6.

Miller, L. A., T. N. Papakyriakou, R. E. Collins, J. W. Deming, J. K. Ehn, R. W. Macdonald, A. Mucci, O. Owens, M. Raudsepp, and N. Sutherland (2011), Carbon dynamics in sea ice: A winter flux time series, *J. Geophys. Res.*, *116*, C02028, doi:10.1029/2009JC006058.

Millero, F. J. (1995), Thermodynamics of the carbon dioxide system in the oceans, *Geochim. Cosmochim. Acta*, *59*, 661–677, doi:10.1016/0016-7037(94)00354-O.

Millero, F. J., and A. Poisson (1981), International one-atmosphere equation of state of seawater, *Deep Sea Res., Part A*, *28*, 625–629, doi:10.1016/0198-0149(81)90122-9.

Munro, D. R., R. B. Dunbar, D. A. Mucciarone, K. R. Arrigo, and M. C. Long (2010), Stable isotopic composition of dissolved inorganic carbon and particulate organic carbon in sea ice from the Ross Sea, Antarctica, *J. Geophys. Res.*, *115*, C09005, doi:10.1029/2009JC005661.

Norman, L., D. N. Thomas, C. A. Stedmon, M. A. Granskog, S. Papadimitriou, R. H. Krapp, K. M. Meiners, D. Lannuzel, P. van der Merwe, and G. S. Dieckmann (2011), The characteristics of dissolved organic matter (DOM) and chromophoric dissolved organic matter (CDOM) in Antarctic sea ice, *Deep Sea Res., Part II*, *58*, 1075–1091, doi:10.1016/j.dsr2.2010.10.030.

Papadimitriou, S., H. Kennedy, G. Kattner, G. S. Dieckmann, and D. N. Thomas (2004), Experimental evidence for carbonate precipitation and CO_2 degassing during sea ice formation, *Geochim. Cosmochim. Acta*, *68*, 1749–1761, doi:10.1016/j.gca.2003.07.004.

Papadimitriou, S., D. N. Thomas, H. Kennedy, C. Haas, H. Kuosa, A. Krell, and D. S. Dieckmann (2007), Biogeochemical composition of natural sea ice brines from the Weddell Sea during early austral summer, *Limnol. Oceanogr.*, *52*, 1809–1823, doi:10.4319/lo.2007.52.5.1809.

Papadimitriou, S., D. N. Thomas, H. Kennedy, H. Kuosa, and G. S. Dieckmann (2009), Inorganic carbon removal and isotopic enrichment in Antarctic sea ice gap layers during early austral summer, *Mar. Ecol. Prog. Ser.*, *386*, 15–27, doi:10.3354/meps08049.

Perovich, D. K., and A. J. Gow (1996), A quantitative description of sea ice inclusions, *J. Geophys. Res.*, *101*, 18,327–18,343, doi:10.1029/96JC01688.

Petrich, C., and H. Eicken (2010), Growth, structure and properties of sea ice, in *Sea Ice*, 2nd ed., edited by Thomas D. N. and G. S. Dieckmann, pp. 23–77, Wiley-Blackwell, Oxford, U. K.

Pringle, D. J., H. J. Trodahl, and T. G. Haskell (2006), Direct measurement of sea ice thermal conductivity: No surface reduction, *J. Geophys. Res.*, *111*, C05020, doi:10.1029/2005JC002990.

Redfield, A. C., B. H. Ketchum, and F. A. Richards (1963), The influence of organisms on the composition of sea-water, in *The Sea*, vol. 2, edited by M. N. Hill, pp. 26–77, Interscience, New York.

Ricker, W. E. (1973), Linear regressions in fishery research, *J. Fish. Res. Board Can.*, *30*, 409–434, doi:10.1139/f73-072.

Rysgaard, S., J. Bendtsen, B. Delille, G. S. Dieckmann, R. N. Glud, H. Kennedy, J. Mortensen, S. Papadimitriou, D. N. Thomas, and J. L. Tison (2011), Sea ice contribution to the air-sea CO_2 exchange in the Arctic and Southern Oceans, *Tellus, Ser. B*, *63*, 823–830, doi:10.1111/j.1600-0889.2011.00571.x.

Tison, J. L., T. Worby, B. Delille, F. Brabant, S. Papadimitriou, D. N. Thomas, J. de Jong, D. Lannuzel, and C. Haas (2008), Temporal evolution of decaying summer first-year sea ice in the western Weddell Sea, Antarctica, *Deep Sea Res., Part II*, *55*, 975–987, doi:10.1016/j.dsr2.2007.12.021.

Toggweiler, J. R., and B. Samuels (1995), Effect of sea ice on the salinity of Antarctic bottom waters, *J. Phys. Oceanogr.*, *25*, 1980–1997, doi:10.1175/1520-0485(1995)025<1980:EOSIOT>2.0.CO;2.